



## Numerical Simulation of Velocity Distribution in the River Lateral Intake Using the SSIIM2 Numerical Model

Adel ASNAASHARI<sup>1</sup>, Edris MERUFINIA<sup>1,\*</sup>

<sup>1</sup>Young Researchers and Elite Club, Mahabad Branch, Islamic Azad University, Mahabad, Iran

Received: 01.02.2015; Accepted: 05.05.2015

**Abstract.** Intakes are generally used in water distribution networks, irrigation channels, sewage networks, water, and wastewater treatment facilities as an input to power utilities, and so on. Due to the flow complexity and also the Effects of scale, physical models can not solely provide a clear perception of the physics governing the flow field and it is necessary to study this phenomenon numerically along with field and Experimental studies. In the first section of this study, the numerical simulation of flow has been performed in the direct path of rectangular channel by Using SSIIM2 software. This software solves Navier-Stokes equations by Finite-Volume Method (FVM). The flow calculations were performed in the three dimensional model using K- $\epsilon$ -RNG and K- $\epsilon$ -Standard turbulence models. The K- $\epsilon$ -Standard turbulence model showed the best results according to the comparison of velocity profiles with the experimental results of Barkdollet al. (1998) and the results of other numerical studies. Then, in the second section, using this turbulence model, the flow velocity profiles at different sections of the main channel and Intake were compared with the experimental and numerical results of other researchers; and a good agreement has been found between them. The comparison of the obtained results with experimental and numerical results of other researchers indicates that this numerical model can well predict the flow velocity profile in the different sections of the main channel and intake. Given the satisfactory results obtained from the above comparisons, the last section presents a numerical study of other parameters such as shear stress and pressure distribution in the main channel and intake.

**Keywords:** lateral intake, flow velocity profile, shear stress and pressure distribution, SSIIM2

### 1. INTRODUCTION

Diversion of water from its main rout has been done since the past time for many purposes such as agriculture, urban water supply, etc. The diverted flow into the intake has complex characters and leads to the formation of separation zones in the main channel and intake. The flow stream that pours into the basin has a very strong momentum in the direction of the main Channel and therefore the flow separation occurs in the basin.

In this area, the fluid particles have spinal movement in the left side of the basin Chanel and in fact, this region of Channel has no effect on the discharge rate of the flow. In other words, the flow separation zone reduces the intake flow and increases the velocity in other parts of the flow. Also due to changes in the velocity distribution in the region, sedimentation occurs in the inlet of the intake that leads to reduction of intake efficiency, the inlet of coarse sediments and increased administrative costs for sediment removal. Any action that reduces the secondary flow and vortex at the inlet causes decreased accumulation of sediment in the inlet and reduced amount of sedimentation in the intake. Many studies are done on the diversion of direct path of flow by previous scholars [1].

Law and Reynolds (1966) performed an analytical and experimental study on the main and lateral channel with equal width and provided an equation for the ratio of discharge and different Froude number before and after the intersection and width ratio of the two channels [2].

\*Corresponding author. Email address: edris.marufynia@yahoo.com

Chen & Lian (1992) simulated the geometry of T-shaped Intersection which was studied by Pope and Salt in 1983 in two dimensional forms by using the standard K- $\epsilon$  model along with the above Reynolds numbers. The obtained results for relatively small flows were consistent with previous experimental measurements. But in a larger proportion of discharges, their prediction was fundamentally different from the measurements [3].

Kasthuri and Pundarikanthan (1987) performed an experimental study on measuring the length and width of rotation region in 90° branch of a rectangular channel and concluded that the dimensions of water flow separation zone varying in proportion to the increase in dewatered, length and width of the vortex at the inlet of the intake channel is reduced [4].

Ramamurthy et al. (2007) conducted a laboratory study in a 90° intake of a rectangular cross-section and used 3D tools to measure the velocity at different sections [5].

Issa and Oliveira (1994) performed Three-dimensional simulation of turbulent flow in T-shaped geometries. They solved the time-averaged Navier-Stokes equations by Reynolds method in three-dimensional mode (RANS) along with the Standard k- $\epsilon$  model with wall functions. In this case, the equations were solved using the finite volume method with an accuracy of the first order [6].

Neary et al. (1996) studied the multi-layer flow pattern in 90 ° branch through developing a three-dimensional numerical model. The researchers used the finite volume method for solving equations and were able to investigate the flow pattern in the field and simulate the quality movement of bed load sediments [7].

Shamloo & Pirzadeh (2008) conducted the Numerical study of flow hydraulics in River lateral intakes by using Fluent software. In this study, the 3D measurement of velocity profiles was done through the K- $\epsilon$ -Standard turbulence model and there were a good agreement between the estimated and experimental results [8].

Goudarzizadeh, et al (2010) studied the three dimensional numerical analysis of the flow pattern in the basin of the direct route by using finite volume method In this study, velocity profiles at different sections of the main channel and the basin were analyzed by using K- $\epsilon$ -RNG turbulence model and the results were compared with experimental results [9].

Shafaeibajestan et al (2011) conducted the Experimental and numerical study of the flow pattern in 30 degrees basin branching from a trapezoidal channel. In the study, different experiments were performed in a laboratory flume on a 30-degree angle on the side basin derived from the trapezoidal channel and the 3D components velocity was measured. Then the SSIIM2 was calibrated and validated using this data. The results showed that the separated flow width on the floor and surface are directly related to the level of intake. It was also shown that in comparison with intake of the direct channel, the width of the trapezoidal channel is increased at surface and reduced on the floor and since the density of the sediments is higher than surface layers; the inclined wall of the main channel causes the reduction of input sediment [10].

Mohammedans et al (2013) examined the effect 90 degrees rounded bottom edge of the direct and the arched shape channels on the flow pattern. In our study, the modification of flow pattern and the reduction of erosion and sedimentation were evaluated through replacing the downstream vertical edge intersection with an arc. The results show that using the arc with that radius has substantially reducing effect of the potential of sedimentation and stream channel erosion [11].

Seyedian and Shafaeibajestan (2011) discussed and evaluated determination of the size and strength of the vortex spiral flow at lateral intakes. In this study some experiments were

## Numerical Simulation of Velocity Distribution in the River Lateral Intake Using the SSIIM2 Numerical Model

performed in a laboratory flume with side intake of 90 degrees angle and the three-dimensional components of velocity were measured and these data were used for calibration and validation of mathematical models SSIIM2 and this model was run for other hydraulic conditions to obtain an acceptable range of the data. The results showed that the separated flow width on the floor and surface are directly related to the level of intake. Also the power of the secondary flow at the beginning of the basin that affects the transfer of the load to the surface was calculated which is inversely proportional to the Froude number and directly related to the ratio of intake [12].

Shakibainia et al. (2008) analyzed the use of three-dimensional numerical modeling for the simulation of complex river engineering phenomena by using SSIIM2 model [13].

Karami Moghadam et al (2006) analyzed the evaluation of rounded radius in the intersection of the separation zone through SSIIM2 3D model, and the results were verified by physical methods [14].

Montaser et al (2008) through using the flow pattern in front of the intake showed that In a 180 degree arc the front of the intake flow is higher in the upper layer than the lower layer and it decreases near the surface. Also the maximum strength of the secondary flow exists in 45 ° cross section of the arc and there is also a relative maximum at 130° [15].

The purpose of this study was analyzing the efficiency of three-dimensional numerical models in river engineering problems and their verification in some complicated cases. The results of numerical model were compared with experimental or field results. The results of the study imply to the high ability of the numerical model that can be used for solving river engineering problems.

## 2. MATERIAL AND METHODS

### 2.1. SSIIM2 numerical software and the equations

SSIIM2 software was designed for simulation of sedimentation and hydraulic study of pools and rivers. This software solves Navier-Stokes equations using the finite volume method for three-dimensional (Finite-Volume Method). Finite volume method is based on direct discretization of the integral formulation of conservation laws based on physical space. Flow analysis has been conducted in steady position and the SIMPLE algorithm is used for pressure velocity coupling. Discretization method of the momentum equation, drop and turbulent kinetic energy and Reynolds stress is the second order and the differencing method for pressure equation is the standard method. The turbulence models used in this application include turbulence model K-ε-standard, turbulence model K-ε-RNG, turbulence model k-ε based on water velocity, turbulence model k-ω with the terms of the walls of Wilcox's and the turbulence model k-ω along with laws of wall k-epsilon.

Regarding the differential shape of the survival law,  $\frac{\partial U}{\partial t} + \vec{\nabla} \cdot \vec{F} = Q$  the important step in the method of infinite volume is the integration of the equations that govern the controlled volume.

$$\int_{\Omega_J} \frac{\partial U}{\partial t} d\Omega + \int_{\Omega_J} \vec{\nabla} \cdot \vec{F} d\Omega = \int_{\Omega_J} Q d\Omega \quad (1)$$

Based on the Gauss divergence theorem:

$$\int_{\Omega_j} \vec{\nabla} \cdot \vec{F} d\Omega = \int_S \vec{F} \cdot d\vec{S} \quad (2)$$

The Integral form of survival law ref for the controlled volume of  $\Omega_j$  at point J will be:

$$\frac{\partial}{\partial t} \int_{\Omega_j} U d\Omega + \int_{S_j} \vec{F} \cdot d\vec{S} = \int_{\Omega_j} Q d\Omega \quad (3)$$

The above equation is replaced by its discrete form where the integral volume is stated as Buffering and integral values on the cell surface of the target volume as a total package.

$$\frac{\partial}{\partial t} (U_j \Omega_j) + \sum_{faces} \vec{F} \cdot \Delta \vec{S} = Q_j \Omega_j \quad (4)$$

The equations that govern the fluid movement include: the continuity equation and momentum equation for turbulent flow in incompressible fluid in a three-dimensional geometries mentioned in equations (5) and (6), respectively. In different turbulence models, the turbulent kinetic energy according is defined by Equation (7).

$$\frac{\partial \bar{U}_i}{\partial x_i} = 0 \quad (5)$$

$$\frac{\partial \bar{U}_i}{\partial t} + (\bar{U}_j) \frac{\partial \bar{U}_i}{\partial x_j} = -\frac{1}{\rho} \frac{\partial p}{\partial x_i} + g_{xi} + \frac{\partial}{\partial x_j} [v \frac{\partial \bar{U}_i}{\partial x_j} - \overline{U'_i U'_j}] \quad (6)$$

$$K = \frac{1}{2} \overline{U_i U_j} \quad (7)$$

Where  $\rho \bar{u}_i \bar{u}_j$  refers to Reynolds stress,  $U_i$  and  $U_j$  refer to the flow velocity in the x and y, t refers to time,  $\nu$  is molecular viscosity, p is pressure, K is turbulent kinetic energy Reynolds stresses, respectively, the flow velocity in the x and y, t time,  $\nu$  molecular viscosity, p the pressure, k turbulent kinetic energy,  $\rho$  the fluid density and  $g_{xi}$  refers to the gravitational acceleration on  $x_i$  direction.

In The turbulence model k-ε, turbulent kinetic energy (k) is as follows:

$$\frac{\partial k}{\partial t} + U_j \frac{\partial k}{\partial x_j} = \frac{\partial}{\partial x_j} \left( \frac{V_T}{\sigma_k} \frac{\partial k}{\partial x_j} \right) + P_k - \varepsilon \quad (8)$$

$P_k$  is calculated as follows:

$$P_k = \nu_T \frac{\partial U_j}{\partial x_i} \left( \frac{\partial U_j}{\partial x_i} + \frac{\partial U_i}{\partial x_j} \right) \quad (9)$$

## Numerical Simulation of Velocity Distribution in the River Lateral Intake Using the SSIIM2 Numerical Model

$$v_T = c \mu \frac{K}{\varepsilon^2} \quad (10)$$

K is marked as  $\varepsilon$  as follows:

$$\frac{\partial \varepsilon}{\partial t} + U_j \frac{\partial \varepsilon}{\partial x_j} = \frac{\partial}{\partial x_j} \left( \frac{v_T \partial \varepsilon}{\sigma_k \partial x_j} \right) + C_{\varepsilon 1} \frac{\varepsilon}{k} P_k + C_{\varepsilon 2} \frac{\varepsilon^2}{k} \quad (11)$$

In the above equation,  $P_k$ , turbulence production term and experimental values of the constants used are as follows:

$$C_{\mu} = 0.09, C_{1\varepsilon} = 1.43, C_{2\varepsilon} = 1.92, \sigma_{\varepsilon} = 1.3, \sigma_k = 1 \quad (12)$$

### 2.2. The characteristics of Barkdoll et al (1998) experimental model

In Barkdoll et al (1998) experimental model the lengths of the main and lateral channel's are 2.74 and 1.68 m respectively. The intake angle is  $90^\circ$  and the cross sections are rectangular. The inflow to the main channel ( $Q_1$ ) is 0.011m/s, the depth ( $d$ ) is 0.31 m. Discharge ratio is 0.31, Reynolds number ( $Re$ ) is 49600 and width of the both channels ( $b$ ) are 0.152m [16]. Figure (1) shows a design of the channel and it's the hydraulic characters are listed in Table (1).

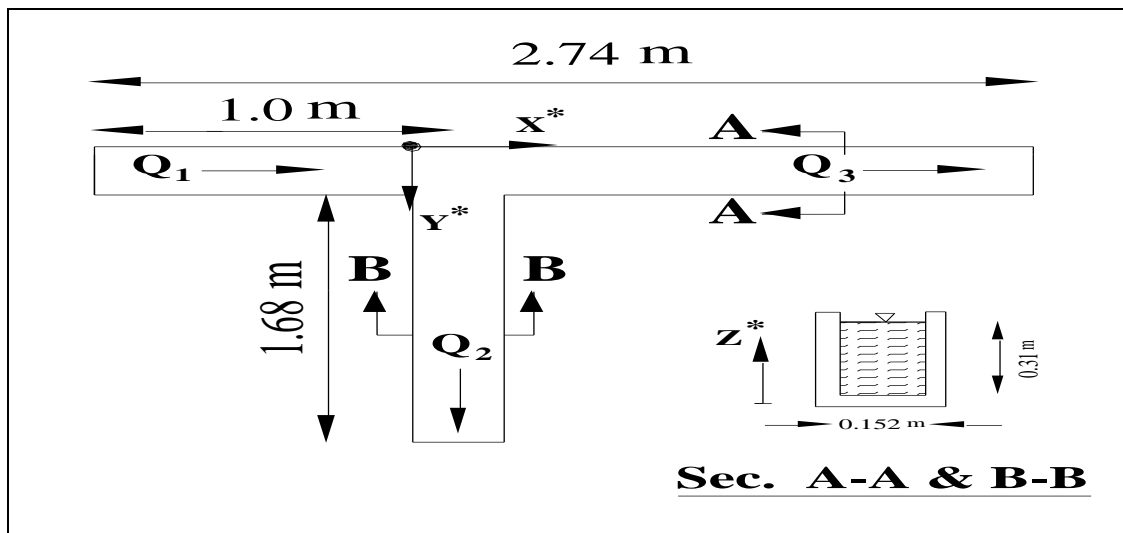


**Figure 1.** Geometric properties of laboratory flume.

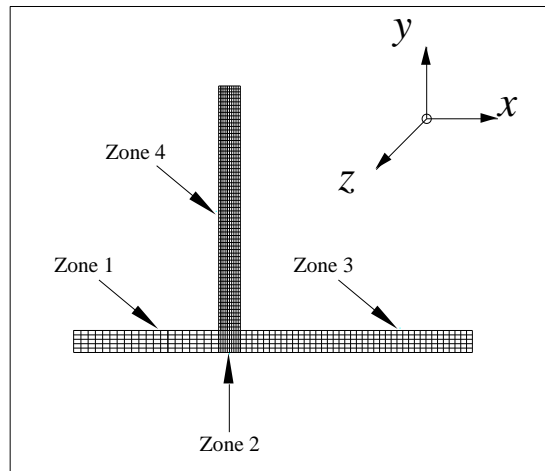
**Table 1.** The hydraulic characteristics of flow.

| D(m) | Q <sub>1</sub> (Lit/s) | R     | Q <sub>3</sub> (Lit/s) | Q <sub>2</sub> (Lit/s) | Re    | Fr          |
|------|------------------------|-------|------------------------|------------------------|-------|-------------|
| 0.31 | 11                     | 0.311 | 7.95                   | 3.41                   | 49600 | <b>0.13</b> |

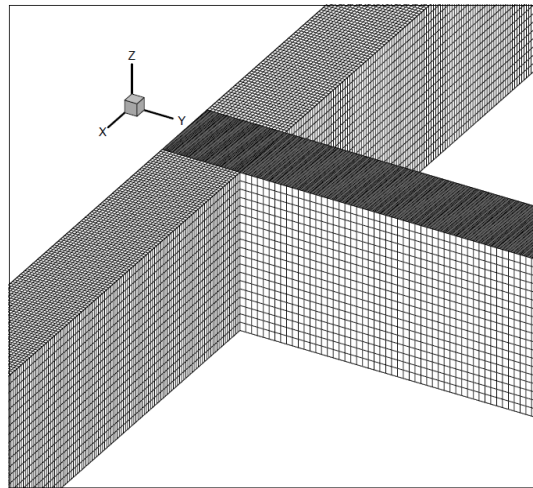
### 2.3. Meshing and computational boundary conditions for simulation of Barkdoll et al

#### 2.3.1. Experiments

In this study, velocity inlet boundary condition has been specified and set to 0.236 m/s. The ratio of intake discharge (R) regarding the amount of the experimental model is 0.31. Regarding small changes in water level, the symmetry boundary condition is applied to the surface. The wall boundary condition is applied to the rigid boundaries and hydraulically smooth walls. Also one of the important parameters which are effective on speed of performing the model is the suitable district networking in which the flow is established. Figure (2) represents Meshing of the computational field in 90° intake. The numbers and dimensions of the cells at x,y, and z directions are listed in Table (2).



a



b

**Figure 2.** Meshing of the computational field in plan (a) and (b) 3D.

## Numerical Simulation of Velocity Distribution in the River Lateral Intake Using the SSIIM2 Numerical Model

**Table 2.** The numbers and dimensions of the cells of the field in different directions

| Zone   | Number of the cells in x direction | Number of the cells in y direction | Number of the cells in z direction | Dimensions of the cells in x(mm) | Dimensions of the cells in y (mm) | Dimensions of the cells in z(mm) |
|--------|------------------------------------|------------------------------------|------------------------------------|----------------------------------|-----------------------------------|----------------------------------|
| Zone 1 | 25                                 | 120                                | 19                                 | 7.70                             | 6                                 | 16.31                            |
| Zone 2 | 25                                 | 50                                 | 19                                 | 6                                | 3                                 | 16.31                            |
| Zone 3 | 25                                 | 240                                | 19                                 | 6.93                             | 6                                 | 16.31                            |
| Zone 4 | 150                                | 50                                 | 19                                 | 3                                | 11.20                             | 16.31                            |

### 2.4. The characteristics of Shettar and Murthy (1996) experimental model

In Shettar and Murthy (1996) experimental model the lengths of the main and lateral channel are 6 and 3 m forming a 90° angle. The inflow to the main channel is 0.063m/s, the depth (d) is 0.25 m. width of the both channels (b) is 0.3m and the Freud number of inflow is 0.54 [17]. Figure (3).

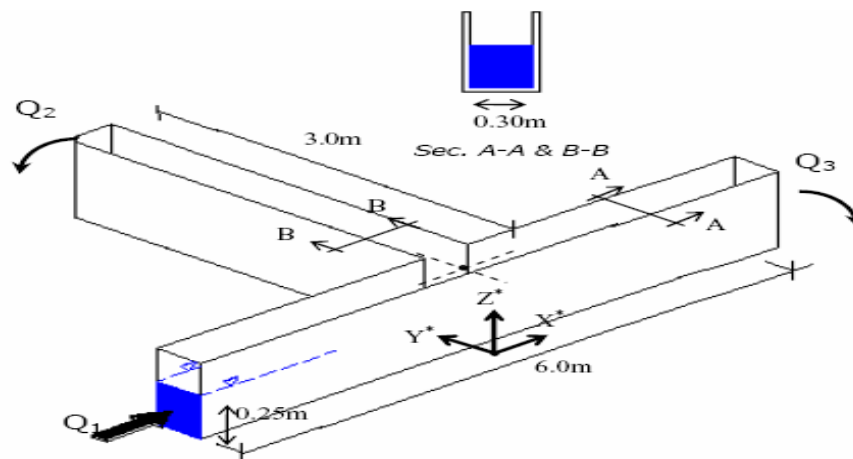


**Figure 3.** Geometric properties of laboratory flume

### 2.5. Meshing and computational boundary conditions for simulation of Shettar and Murthy (1996) experiments

The wall boundary condition of this part is the same as before and Constant velocity boundary condition at the inlet channel is considered 0.85 meters per second. The ratio of diverted discharge (R) regarding the amount of the experimental model is 0.52. Table 3 represents the number and dimensions of the cells of the field in different directions of x,y and z.

**Table 3.** The number and dimensions of the cells of the field in different directions

| Zone   | Number of the cells in x direction | Number of the cells in y direction | Number of the cells in z direction | Dimensions of the cells in x(mm) direction | Dimensions of the cells in y(mm) | Dimensions of the cells in z(mm) |
|--------|------------------------------------|------------------------------------|------------------------------------|--|----------------------------------|----------------------------------|
| Zone 1 | 25                                 | 150                                | 19                                 | 19   | 12                               | 13.15                            |
| Zone 2 | 25                                 | 50                                 | 19                                 | 6  | 12                               | 13.15                            |
| Zone 3 | 25                                 | 150                                | 19                                 | 19   | 12                               | 13.15                            |
| Zone 4 | 25                                 | 50                                 | 19                                 | 6  | 20                               | 13.15                            |

### 3. RESULTS AND DISCUSSIONS

#### 3.1. Comparing the velocity profiles in the numerical with Barkdoll et al. models

The velocity profiles have become non-dimensional in fig.4 ( $U_x/U_0$ ) near the surface, for different cross sections of the main channel for 0.011 m/s fixed-rate input, The ratio of intake discharge (R) 0.31 and the Froud number of the inflow 0.13 (Fr).  $X^*$ ,  $Y^*$  are the distance at x & Y axes respectively which have become non-dimensional through the basin width (b).  $U_x$  is the maximum velocity at  $X^*=-3.93$  which equals to 0.28 m/s.

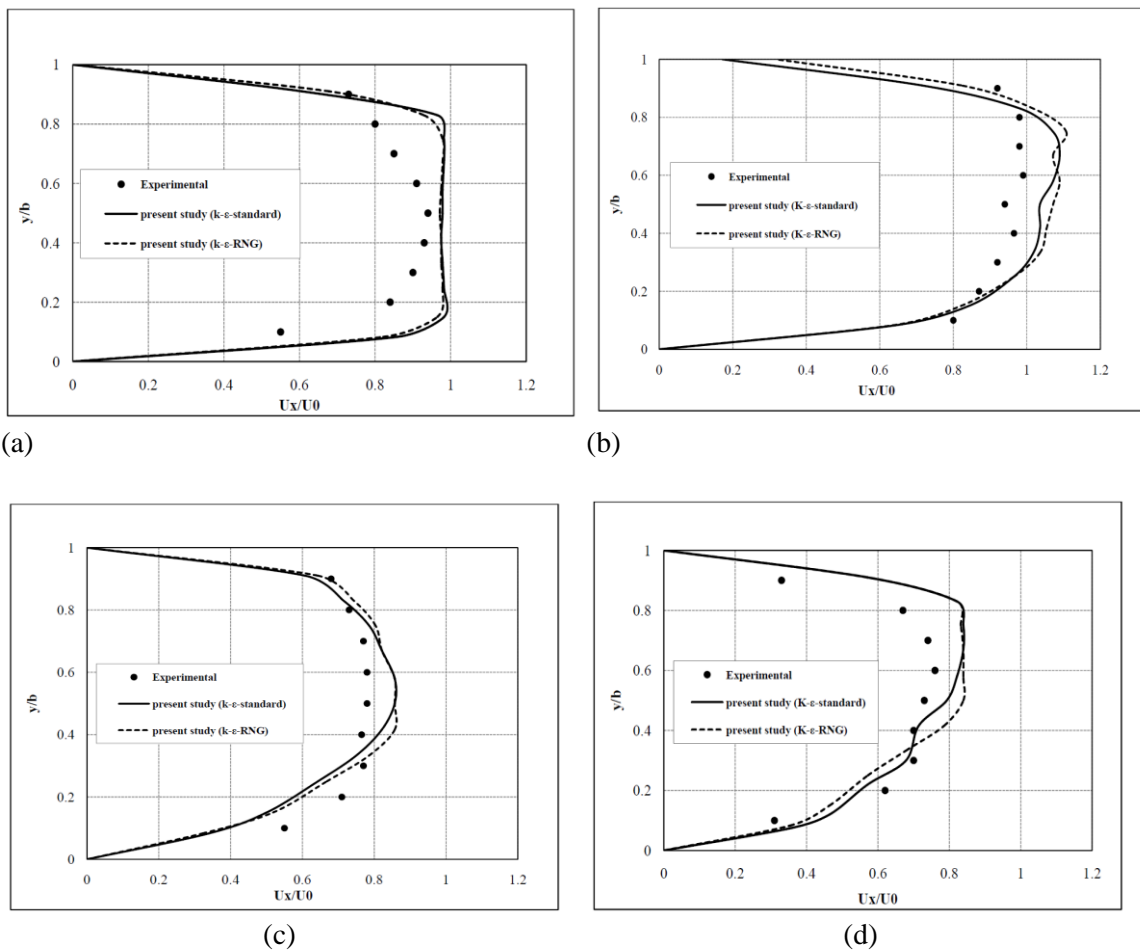


**Figure 4.** The analysis of velocity profiles at different sections of the main channel  $X^*=3.93$  (a)  $X^*=0.49$  (b),  $X^*=0.51$  (c) and  $X^*= 2.01$  by using different turbulent models

## Numerical Simulation of Velocity Distribution in the River Lateral Intake Using the SSIIM2 Numerical Model

According to Figure (4-a), velocity profile prior preserves its expanded state until it gets into the basin inlet. And by approaching the inlet, due to the intake suction of the intake, velocity profiles bend toward the branching channel and the maximum velocity switch into the inlet (point  $X^* = -0.49$ ) (Figure 4-b). The results of this study indicated that with the entrance of the flow into the intake the resultant velocity has decreased over the inlet and at the downstream side of the inlet (point  $X^* = 0.51$ ) and the maximum velocity gets away from the inside wall of the main channel. The residual flow after passing the inlet extends in the section and due to the effect resulting from Curvature flow in the inlet lines the maximum velocity is deflected towards the inner wall. The value of predicted numbers is greater than the experimental value which is due to ignoring the effect of the tension in the air in numerical modeling. The velocity profiles have become non-dimensional in Figure (5). ( $U_y/U_0$ ) near the surface, for different cross sections of the main channel. The numerical results from Fluent software are obtained by the numerical study Safarzadeh and Neishabouri (2004) in which in order to analyze the distribution of flow velocity the K- $\epsilon$ -Standard is used. Also the numerical results of Finite-Volume are obtained from Goudarzizade et al (2010) studies in which the K- $\epsilon$ -RNG turbulent model is used.

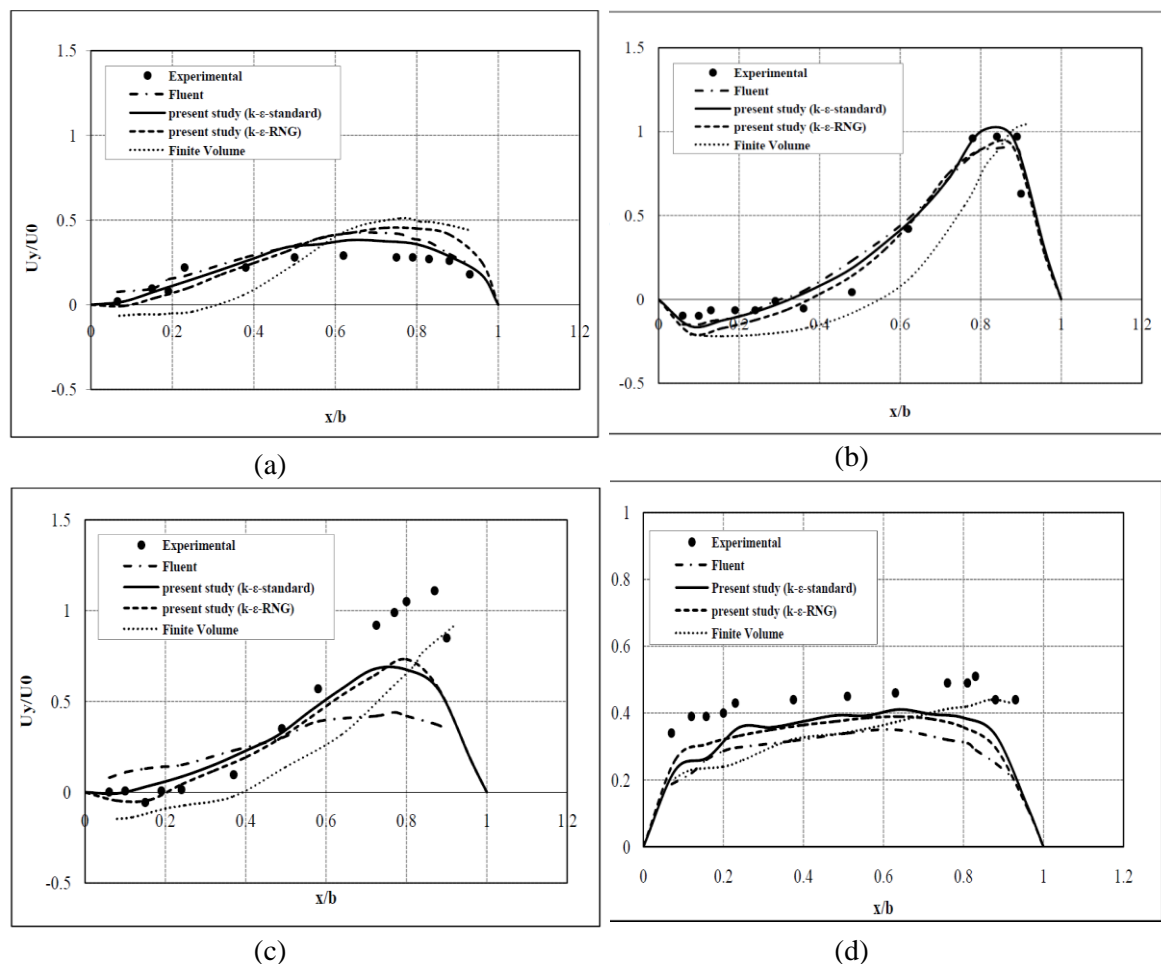


**Figure 5.** The analysis of velocity profiles at different sections of the main channel  $Y^*=1$  (a)  $Y^*=2.5$  (b),  $Y^*=4$  (c) and  $Y^*=10$  by using different turbulent models

According to Figure (5-b) due to the separation zone which is formed at the beginning of the basin the relative speed is negative. Also in Figure (5-a), because the flow has not entered into the separation zone, the relative velocity is not negative. According to Figure(4) and (5) the K-

$\epsilon$ -standard turbulent model has a better performance in estimating velocity than K- $\epsilon$ -RNG turbulence model and the Positive and negative values of velocity in the channel match with the experimental model. The value of predicted numbers is greater than the experimental value which is due to the effects of the secondary flow that transfer the velocity into the lower levels. Table (4) represents the mean percentage error obtained from comparing the numerical values of SSIIM2 and Fluent with experimental data at different levels of the main channel and intake.

**Table 4.** The mean percentage error obtained from comparing the numerical values of velocity profile at different sections of the two channels with experimental values

| Section                          | X*    |       |       |       | Y*    |       |       |       |
|----------------------------------|-------|-------|-------|-------|-------|-------|-------|-------|
|                                  | -3.93 | -0.49 | 0.51  | 2.01  | 1     | 2.5   | 4     | 10    |
| SSIIM2 (K- $\epsilon$ -Standard) | 13.28 | 9.67  | 12.30 | 10.71 | 5.73  | 15.25 | 20.60 | 9.14  |
| SSIIM2 (K- $\epsilon$ -RNG)      | 13.59 | 10.72 | 13.47 | 11.42 | 11.20 | 20.76 | 22.02 | 10.05 |
| Fluent                           |       |       |       |       | 6.41  | 11.98 | 41.33 | 14.67 |

In the second part of this study, considering the good results obtained in the first part of the study we will analyze buffered velocity profiles of the main channel and basin in experimental model of Shettar and Murthy (1996) by using the K- $\epsilon$ -standard turbulence model.

### 3.2. Comparing the velocity profiles in the numerical and Shettar and Murthy models

In Figure(6) according to the experimental study the buffered velocity profile at depth and direction x ( $U_x$ ) for different cross sections of the main channel for 0.063 m/s fixed-rate input, The ratio of diverted discharge (R) 0.52 and the Freud number of the inflow 0.54 (Fr) are shown. The numerical results of the Fluent software are obtained from Shamloo and Pirzadeh (2008) in which the K- $\epsilon$ -Standard turbulence model is used.

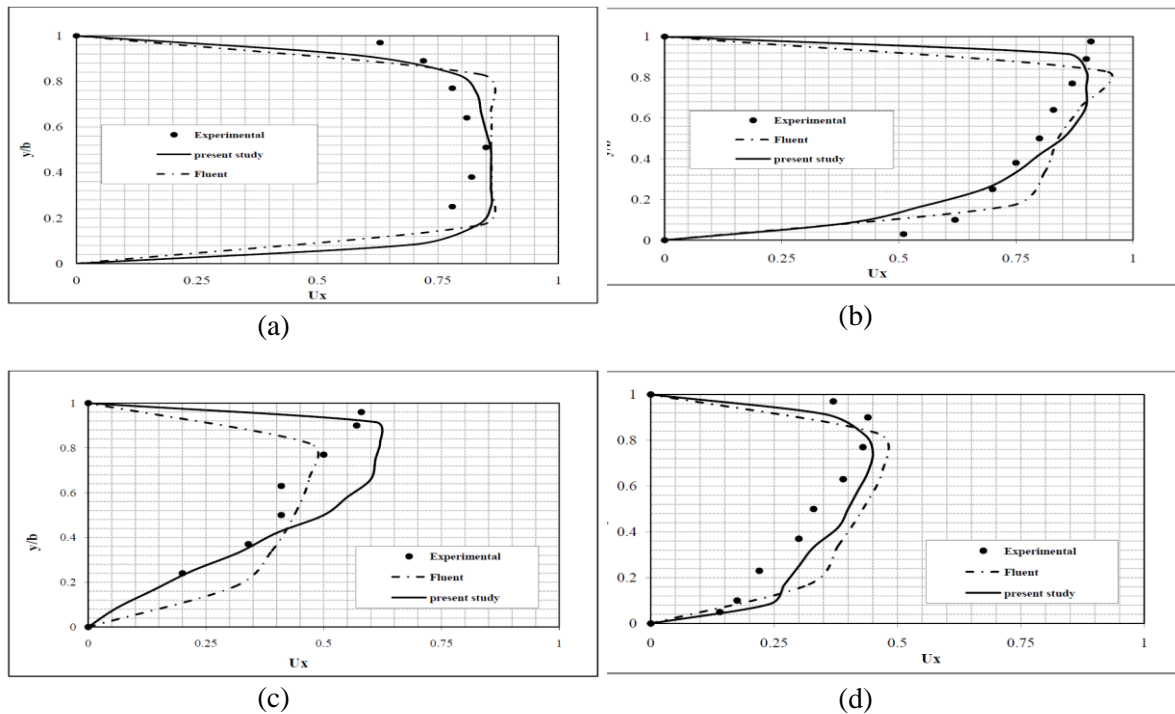


**Figure 6.** The analysis of computational velocity profiles at different sections of the main channel X\*=5.50 (a) X\*=0.05 (b), X\*=1.5 (c) and X\*= 7

## Numerical Simulation of Velocity Distribution in the River Lateral Intake Using the SSIIM2 Numerical Model

According to Figure (6-a), velocity profile prior preserves its expanded state until it gets into the basin inlet. And by approaching the inlet, due to the intake suction of the intake, velocity profiles bend toward the branching channel and the maximum velocity switch into the inlet (Fig 6-b and 6-c) and with the entrance of the flow into the basin. The resultant velocity has decreased over the inlet. Figure (7) shows the buffered velocity profiles in depth and y directions ( $U_y$ ) for different cross sections of the lateral channel.

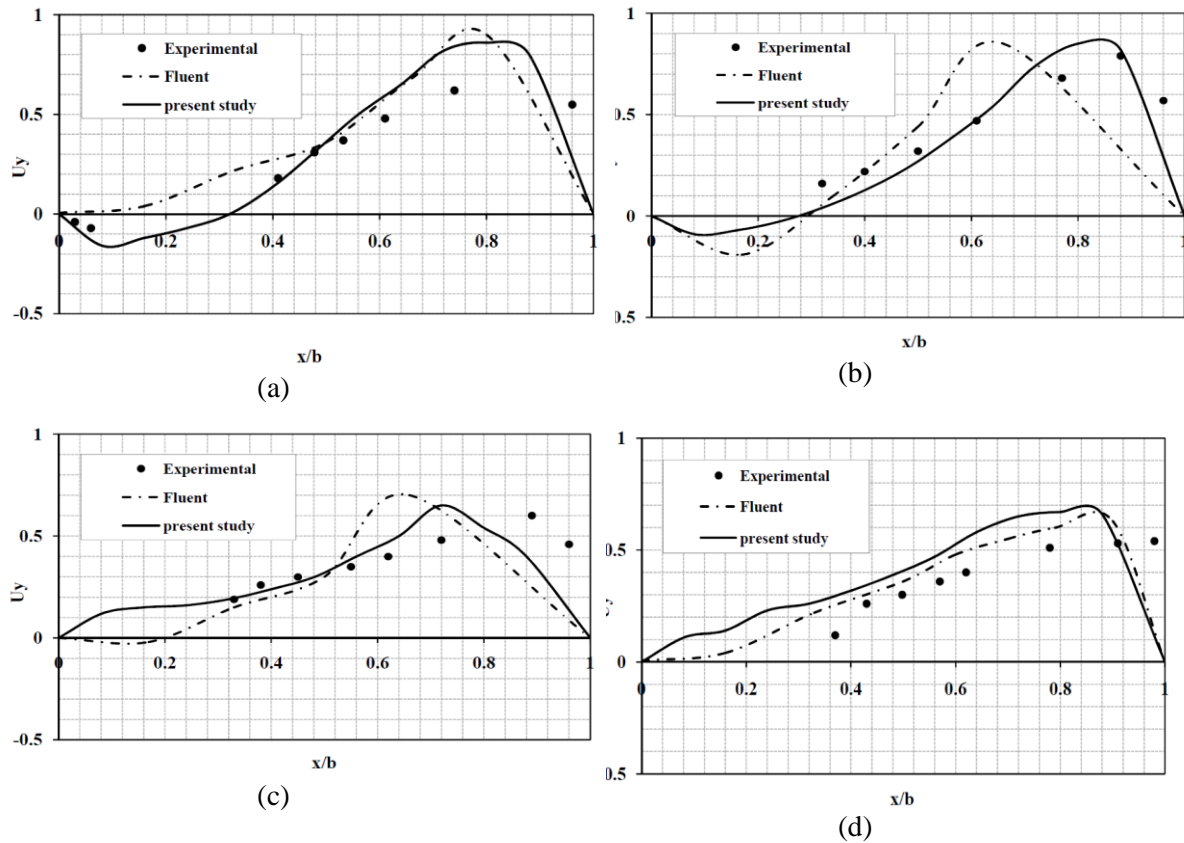


**Figure 7.** The analysis of computational velocity profiles at different sections of the main channel  $Y^*=0.65$  (a)  $Y^*=1.65$  (b),  $Y^*=2.65$  (c) and  $Y^*=3.65$

According to Figures (6) and (7) the K- $\epsilon$ -standard turbulence model has a better performance in estimating velocity and the predicted values are slightly higher than the experimental values. Table (5) represents the mean percentage error obtained from comparing the numerical values of SSIIM2 and Fluent with experimental data at different levels main channel and intake.

**Table 5.** The mean percentage error obtained from comparing the numerical values of velocity profile at different sections of the two channels with experimental values.

| Section                          | $X^*$ |       |       |      | $Y^*$ |      |      |       |
|----------------------------------|-------|-------|-------|------|-------|------|------|-------|
|                                  | -5.50 | -0.50 | 1.50  | 7    | 0.65  | 1.65 | 2.65 | 3.65  |
| SSIIM2 (K- $\epsilon$ -Standard) | 4.47  | 4.67  | 10.15 | 4.65 | 11.46 | 7.66 | 3.55 | 14.33 |
| Fluent                           | 4.98  | 7.48  | 9.03  | 7.60 | 12.57 | 9.04 | 6.87 | 10.42 |

According to the percentage of errors obtained from comparing the numerical values of SSIIM2 with experimental data at different levels they showed better results than fluent numeral model which indicated this models high ability in determining velocity at different sections of the main channel and basin.

### 3.3. The analysis of shear stress and pressure distribution in the main and lateral channels by using numerical models

In the last part based on the good results obtained from the above comparisons and making sure about the high ability of this numerical model we analyze other parameters like shear stress and pressure distribution in the main channel and basin which are not discussed in the experimental results. Fig.8 shows the graphical results (contours) of shear stress and pressure distribution in the main channel and the basin for the discharge 0.011 cubic meters per second, the ratio of diverted discharge 0.31 and inflow Froude number 13.0 in 3d form.

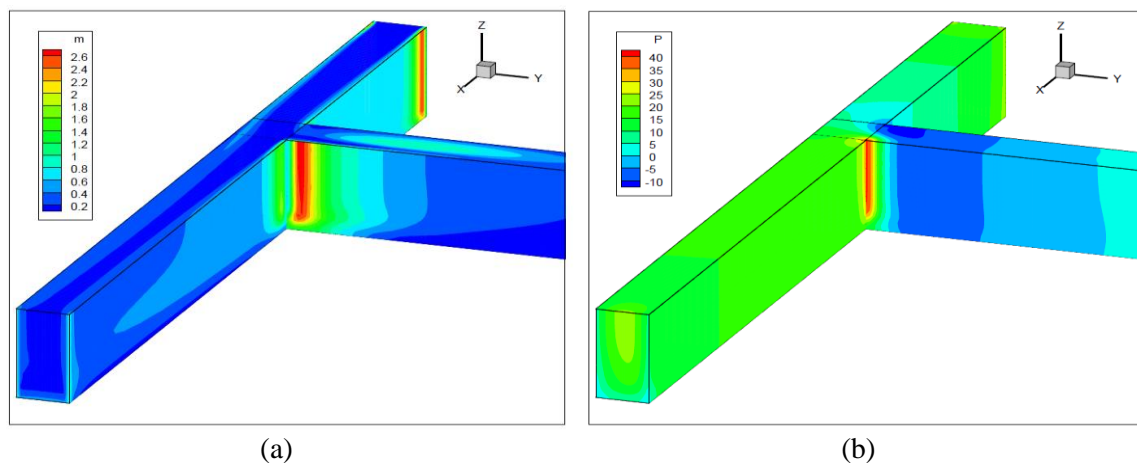


**Figure 8.** The graphical results (contours) of shear stress (a) and pressure distribution (b)

According to (8-a) the maximum shear stress occurs near the downstream wall of the intake channel with the magnitude of 2.6 N m. since the increase in shear stress causes erosion and corrosion on the wall it can be concluded that the risk of corrosion is higher in this region than in other parts. Moreover, according to Figure 8-b, with the entrance into the inlet pressure falls, and when the flow passes through the inlet, the pressure distribution is similar to the distribution of pressure before the intake. The maximum pressure occurs at the top right side of the intake channel which is 39.78 N/m<sup>2</sup>. In Fig.8 the flow direction is toward x axis.

## 4. CONCLUSION

Generally the results of this study include:

➤ The velocity profile preserves its expanded state until it gets into the basin inlet And by approaching the inlet, due to the intake suction of the basin, velocity profiles bend into the branching channel and the maximum speed switch into the inlet (point X \* = 0.51) with the entrance of the flow into the basin the resultant velocity has decreased over the inlet and at the downstream side of the inlet (point X \* = 0.51) and the maximum velocity gets away from the inside wall of the main channel. The residual flow after passing the inlet extends in the section and due to the effect resulting from Curvature flow in the inlet lines the maximum speed is deflected towards the inner wall.

## Numerical Simulation of Velocity Distribution in the River Lateral Intake Using the SSIIM2 Numerical Model

- The K- $\epsilon$ -standard turbulent model has a better performance in estimating velocity than K- $\epsilon$ -RNG turbulence model and the Positive and negative values of velocity in the channel match with the experimental model.
- Both models - regarding the percentage of the errors resulted from comparing the experimental results with the numerical values of SSIIM2 had better performance at most sections than the numerical Fluent model which indicates high ability of the model in determining velocity at different sections of the main and lateral channels.
- The maximum shear stress occurs near the downstream wall of the intake channel with the magnitude of 2.6 N m. since the increase in shear stress causes erosion and corrosion on the wall it can be deduced that the risk of corrosion is higher in this region than in other parts.

### REFERENCES

- [1] Safarzadeh, AS., SalehiNeishabouri, a., (2004), Numerical modeling of flow pattern on the intake side S-h-Bdy, First National Congress on Civil Engineering, Sharif University, Tehran, Iran
- [2] Law, S. W., Reynolds, A. J., (1966)., Dividing flow in an Open Channel. Journal of Hydraulic Engineering. Vol. 92, No. 2, pp. 207-231
- [3] Chen, H. B., and Lian, G. S., (1992)., The Numerical Computation of Turbulent Flow in T-junction. Journal of Hydrodynamics, No.3, pp. 50-58.
- [4] Kasthuri, B., and Pundarikanthan, N.V., (1987)., Discussion on Separation Zone at Open Channel Junction. Journal of Hydraulic Engineering, Vol. 113, No. 4, pp. 543-548.
- [5] Ramamurthy, A.S., Junying, Qu., Diep, V., (2007)., Numerical and Experimental Study of Dividing Open-Channels Flows. Journal of Hydraulic Engineering, Vol. 133, No. 10, pp. 1135-1144
- [6] Issa, R. I., and Oliveira, P. J., (1994)., Numerical Prediction of Phase Separation in Two-Phase Flow Through T-Junctions. Computers and Fluids, Vol. 23, No. 2, pp. 347-372.
- [7] Neary, V.S., Sotiropoulos, F., Odgaard, A. J., (1999)., Three dimensional Numerical Model of Lateral Intake inflows. Journal of Hydraulic Engineering, Vol. 125, No. 2, pp. 126-140.
- [8] Shamloo, H., and Pirzadeh, B., (2008)., Investigation of Characteristics of Separation Zones in T-Junctions. Journal of Wseas Transactions on Applied Mathematics, Vol. 7, No. 5, pp. 303-312.
- [9] Goudarzizadeh, R., Hedayat, N., MousaviJahromi, S.H., (2010)., Three dimensional Simulation of Flow Pattern at the Lateral Intake in Straight Path Using Finite Volume Method. World Academy of Science, Engineering and Technology, pp. 656-661.
- [10] Shafaeibajestan et al, (2011), Experimental and numerical study of the flow pattern 30 degrees split intake of trapezoidal channels, Journal of Science and Technology of Agriculture and Natural Resources, Soil and Water Sciences, Vol XV, Number Fifty-Seven, Iran
- [11] Mohammedans, SA., Salehineyshaboori, a., virtuous, H., Wahhabi, H., (2013), rounded edges at the intersection of 90 degrees down arched channels directly on the flow pattern, The National Conference on Sustainable Development with a focus on Disaster risk Reduction, the institution of higher education rising, Mashhad, Iran
- [12] Sayedian. M, ShafaeiBajestan, d., (2011), the size and strength of the vortex spiral flow at lateral intakes, Journal of Water and Wastewater, No. 4, Isfahan, Iran

- [13] Shakibaiinia A., Zraty, A.r., MajdzadehTabatabai, M.r., (2008), using three-dimensional numerical model for the simulation of complex phenomena River Engineering, College of Engineering, Volume 42, Number 4, page 443 to 455, Tehran, Iran
- [14] KaramiMoghaddam, M., CDs, QM, Shafaeibajestan, d., (2006), the flow pattern in the pond at 90 ° C with inlet roundness SSIIM2 model and comparison with physical modeling, Engineering congress Engineering, Tehran University, Iran
- [15] Montaseri, H., Ghodsian, M., Shafaiefar, M., SalehiNeishabouri, A. A., Dehgahni, A.A. (2008). Experimental investigation of 3D flow field and scouring in a 180 degree bend with a lateral intake.” Gorgan J. of Agri. Sci. and Natural Resources, 15 (2), 225-533.
- [16] Barkdoll, B.D., Hagen, B.L., and Odgaard, A.J.,(1998). Experimental Comparison of Dividing Open Channel with Duct Flow in T-junction. Journal of Hydraulic Engineering. Vol. 124, No. 1, pp. 92-95.
- [17] Shettar, A. S., and Murthy, K. K.,(1996)., A Numerical Study of Division Flow in Open Channels. Journal of Hydraulic Research, Vol. 34, No. 5, pp. 651-675.
- [18] Olsen, N. B. R., (2006)., A Three dimensional Numerical Model for Simulation of Sediment Movements in Water Intakes with Moltiblock Option. Department of Hydraulic and Environmental Engineering, The Norwegian University of Science and Technology